



CuO-Rice Starch Nanocomposites: Synthesis, Characterization and Antibacterial Properties

JAGDISH PRASAD¹, VINOD KUMAR^{2,*}, BHUWAN CHANDRA³, ANSHU TAMTA³, RASHMI KHULBE³ and N.D. KANDPAL³

¹Department of Chemistry, H.S.B. Government PG College, Someshwar-263637, India

²Department of Chemistry, Uttarakhand Open University, Haldwani-263139, India

³Department of Chemistry, Kumaun University, S.S.J. Campus, Almora-263601, India

*Corresponding author: E-mail: drvkumar85@gmail.com

Received: 23 February 2023;

Accepted: 8 April 2023;

Published online: 28 April 2023;

AJC-21225

In current study, the copper oxide-rice starch nanocomposites has been synthesized from the different salts of copper and rice starch. The synthesized nanocomposites were characterized by FT-IR, XRD, SEM, TGA and DSC spectroscopic methods. The spectroscopic analysis showed that the CuO-starch nanocomposite was formed and CuO nanoparticles (CuONPs) were uniformly dispersed in the starch network with relatively smooth surfaces in the CuO-starch nanocomposite. The average crystalline size of CuO-starch nanocomposites from different precursors viz. copper acetate, copper chloride and equimolar mixture of copper acetate and copper chloride were calculated as 3.13 nm, 6.46 nm and 17.42 nm, respectively, while average particle size were 1421, 1504 and 1796 nm, respectively. The TGA and DSC data showed that the CuO-starch nanocomposites were thermally stable. The nanocomposites were scrutinized by antibacterial activity against two tested bacterial strain *Serratia marcescens* (17.67 ± 0.90 mm) and *Escherichia coli* (16.3 ± 0.30). It was concluded that, CuO-starch nanocomposites were thermally stable and exhibited significant antibacterial activity.

Keywords: Copper oxide, Rice-starch, CuO-starch nanocomposites, Antibacterial activity.

INTRODUCTION

Starch has attracted a lot of interest as a biopolymer in recent years due to its benefits, which include low cost, biodegradability, availability, renewability and significant development in non-food and materials applications [1-3]. Nano-sized inorganic and organic fillers are being used to produce a variety of starch-nano biocomposite materials. Enhancement of mechanical, thermal and other properties of nanocomposite materials depends on the geometry, nature and surface chemistry of the nanofiller [4]. The use of metal oxides as antimicrobial agents for starch-based biocomposites is a breakthrough that could potentially help in the food preservation [5].

Copper oxide is most widely used metal oxide in the form of its specific structural properties and its demand in wood preservatives, inks, electronics, films, coating, ceramics and textiles [6]. The synthesis of nanoparticles and nanocomposites of metal oxides is getting attention in biomedical application like antitumor activity [7], antibacterial activity [8] and antimicrobial activity [9] and anticancer activity [10]. The starch has been used as a capping and stabilizing agent for copper

oxide nanoparticles. The starch capped nanoparticles possess chemotherapeutic drug activity for the various types of gastrointestinal cancer namely pancreatic, colon and gastric cancer [11].

In present study, we focus on the synthesis of rice starch-based copper oxide nanocomposite and its characterization by analytical, microscopic along with spectroscopic methods such as SEM, XRD, FT-IR, TGA and DSC. The biological efficacy of the synthesized CuO-starch nanocomposites was achieved by antibacterial activity against selected organisms using ampicillin as standard reference antibiotic.

EXPERIMENTAL

Analytical grade chemicals viz. copper acetate dihydrate [$\text{Cu}(\text{CH}_3\text{COO})_2 \cdot 2\text{H}_2\text{O}$], copper chloride dihydrate ($\text{CuCl}_2 \cdot 2\text{H}_2\text{O}$), glacial acetic acid, sodium hydroxide, acetone, etc. were purchased from Sigma-Aldrich and Merck India. Distilled and deionized water with conductivity less than $1 \mu\text{S cm}^{-1}$ at 25°C was used throughout the experiment for solution preparation and for washing purposes.

Extraction of starch: Rice was purchased from a local source, cleaned and ground into power to extract starch. Starch was extracted by modified alkaline extraction method [12] in which 160 g of rice powder was weighed and 800 mL of 0.05 M NaOH solution was added, then stirred for 3 h at 25 °C and stored overnight at room temperature. The yellow top layer was decanted/separated. Then, blend the residue for 15 min and added 500 mL of 0.05 M NaOH solution for 3 h at 25 °C and store overnight at room temperature. This process was repeated until the yellow layer was completely removed. The alkaline slurry was neutralized with 1.0 M HCl and centrifuged. The resulting starch slurry was washed with 1:1 ratio C₂H₅OH:H₂O and centrifuged again. The obtained starch was dried in a convection oven at 35-40 °C for 48 h and stored in an airtight container for later use.

Synthesis of copper oxide-starch nanocomposites: Copper oxide-starch nanocomposites was synthesized by using different precursors of copper salts solutions 0.2 M CuCl₂·2H₂O, 0.2 M Cu(CH₃COO)₂·2H₂O and equimolar mixture of 0.2 M Cu(CH₃COO)₂·2H₂O and 0.2 M CuCl₂·2H₂O in alkaline medium with some modifications [13] keeping the experimental conditions concentration, pH and temperature unchanged. Starch (4 g) was dissolved in 100 mL of 0.2 M Cu(CH₃COO)₂·2H₂O aqueous solution was placed in a beaker at 80 °C and stirred continuously at 1000 rpm. After reaching thermal equilibrium of 80 °C, 1 mL of glacial acetic acid was added to a beaker that was stirred continuously and steadily using a small magnet at approximately 1000 rpm. Then added 8.0 M NaOH solution dropwise to a copper-starch solution until pH reached 8.5. After the mixture was aged for 30 min under continuous stirring at 80 °C, CuO-starch nanocomposites were obtained. To collect CuO-starch nanocomposites, centrifugation was used at 5000 rpm for 30 min and finally washed with distilled water. The nanocomposites were washed three times with ethanol and acetone and dried at room temperature. Same procedure was followed for the synthesis of CuO-starch nanocomposite from different precursors such as 0.2 M CuCl₂·2H₂O and equimolar mixture of 0.2 M Cu(CH₃COO)₂·2H₂O and 0.2 M CuCl₂·2H₂O.

Characterization: The synthesized rice starch and CuO-starch nanocomposites were characterized using Fourier transfer infrared (FT-IR) spectra recorded at room temperature between 4000-500 cm⁻¹ as KBr pellets using Perkin-Elmer Spectrometer, U.K. The X-ray diffraction (XRD) pattern was measured with a Rigaku, Ultima IV, X-ray diffractometer using CuK α radiation (1.5406 Å) over a scanning range of 10° to 80° with a scanning speed of 8°/min at room temperature. The XRD peaks were recorded at 2 θ the grain size was calculated using the Debye-Scherrer formula. High-resolution images of rice starch and nanocomposites were captured using SEM (EV0 LS10 SEM, Carl Zeiss, Germany). The mean particle size/size distribution and polydispersity index (PDI) were measured using the dynamic light scattering (DLS) RinA, Spectroscatter 201 instrument. Thermal analysis (TGA-DSC) was performed with the help of Setaram, LABSYS DSC 131, 700 °C. The temperature program used was experimentally set from 29 to 400 °C, with a heating rate of 10 °C min⁻¹.

Antibacterial activity: The antibacterial activity of synthesized CuO-starch nanocomposite was performed by

disk-diffusion method against two bacterial strains, *Escherichia coli* (MTCC 443) and *Serratia marcescens* (MTCC 4822) organisms [14]. The test strains were procured from the Institute of Microbial Technology, Chandigarh, India. These bacterial strains were inoculated in the tryptone yeast extract. These strains were incubated for 24 h at 25 °C in the incubator. The tryptone yeast agar plates were prepared with uniform spread out. Each prepared plates were utilized as microbial lawn taking 200 mL of microbial suspension and uniformly spreaded with the help of sterilized spreader. Autoclaved 5.0 mm Whatman filter paper dish (Whatman No. 1) carrying 20 μ L of 5 mg/mL in ethanol of CuO nano-starch nanocomposites were placed on the identified plates. The plates were then incubated for 24 h at 25 °C. The growth of inhibition zones around the sample was measured in diameter.

RESULTS AND DISCUSSION

SEM studies: The surface morphology of the synthesized CuO nanoparticles and CuO-starch nanocomposite was investigated with an scanning electron microscope as shown in Fig. 1a-f. The CuO NPs were spherical in shape, non-uniformly sized, roughly agglomerated and had homogenous morphologies, as seen by SEM micrograph (Fig. 1a). Aggregations between the particles were observed, which might be attributed to the washing stages. Standard starch particles have a smooth, round or oval granular structure, whereas isolated rice starch granules have a homogeneous, polygonal, or polyhedral geometry with average diameters of 20 μ m (Fig. 1b-c). The results of SEM analysis of CuO-starch nanocomposite (Fig. 1d-f) synthesized from the different precursor such as 0.2 M copper acetate, 0.2 M copper chloride and equimolar mixture of copper acetate and copper chloride solution have the average diameters of 10-200 μ m. All the micrographs revealed that CuO NPs were uniformly dispersed in the starch network and relatively smooth surfaces in the CuO-starch nanocomposite. The present finding of the shape, size, morphology and smooth surface of the granules of rice starch indicated that the isolation treatment with 8 M NaOH used in this study did not damage the starch granules was supported with the published data [15-17].

FT-IR studies: The FT-IR spectral data of synthesized CuO-starch nanocomposites are presented in the Table-1. According to FT-IR spectra (Fig. 2a-f), synthesized starch and CuO-starch nanocomposites have an absorption peak between 3299 and 3219 cm⁻¹ that is attributable to the -OH stretching. According to a previous study, the O-H bonds in glucopyranose rings are responsible for the absorption peaks which is observed in all polysaccharides and the vibrational stretching peak breadth indicated that presence of intra- and inter-molecular bonded hydroxyl groups [18]. The other characteristic weak bands were observed at 2901-2885 cm⁻¹ for the synthesized nanocomposites assigned to -CH₂ stretching vibrational. This absorption band occurs due to the asymmetric stretching vibration of the C-CH₂-C in starch. Another band in the spectra of CuO-starch nanocomposites between 2901 and 2885 cm⁻¹ appeared is due to the deformation vibration of the hydroxyl groups of water bonded to the molecules of starch [19]. In the synthesized nanocomposites, another weak band of C-H and O-H bending is

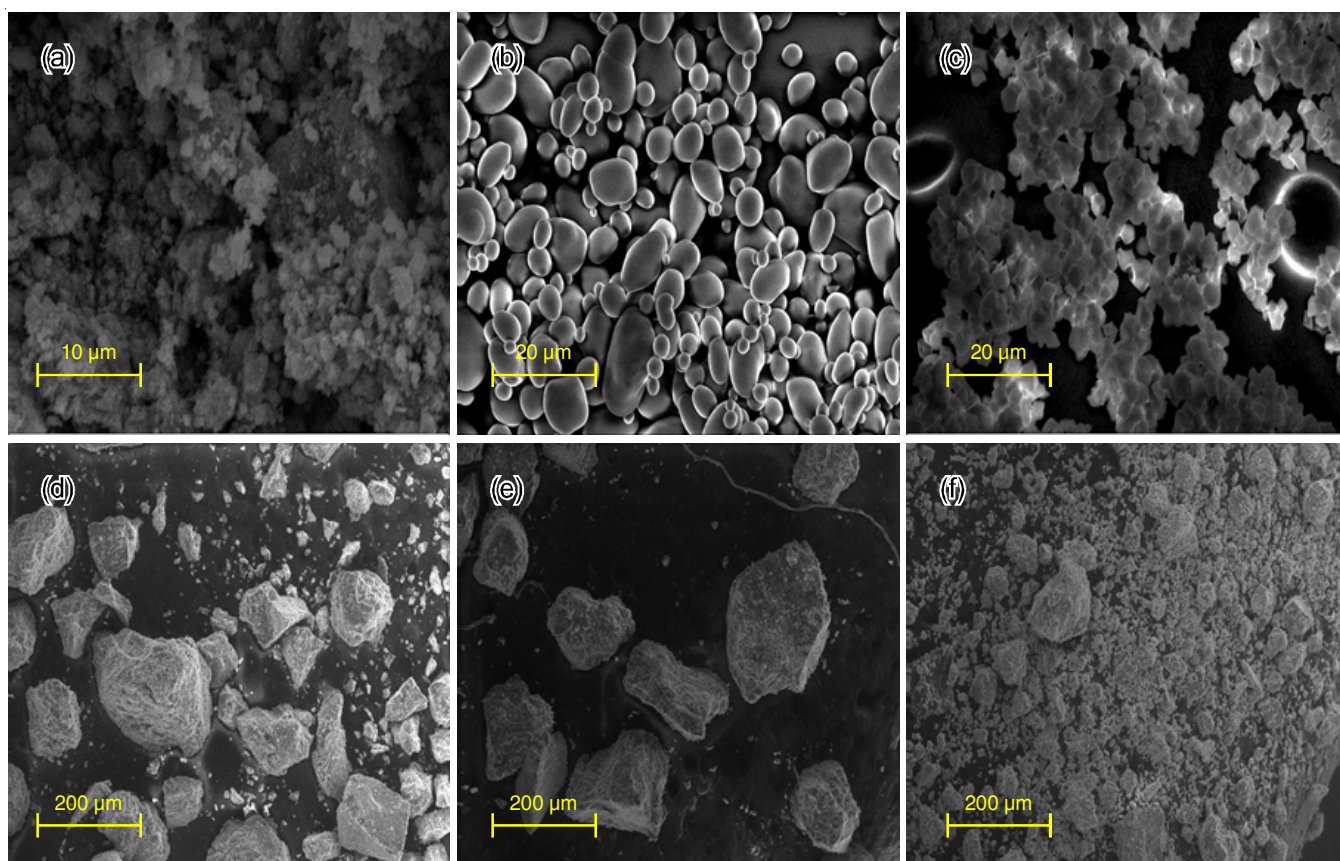


Fig. 1. SEM micrographs of (a) CuO nanoparticles; (b) standard starch; (c) rice starch and (d) CuO-starch nanocomposites from copper acetate; (e) CuO-starch nanocomposites from copper chloride and (f) CuO-starch nanocomposites from equimolar mixture of copper acetate and copper chloride

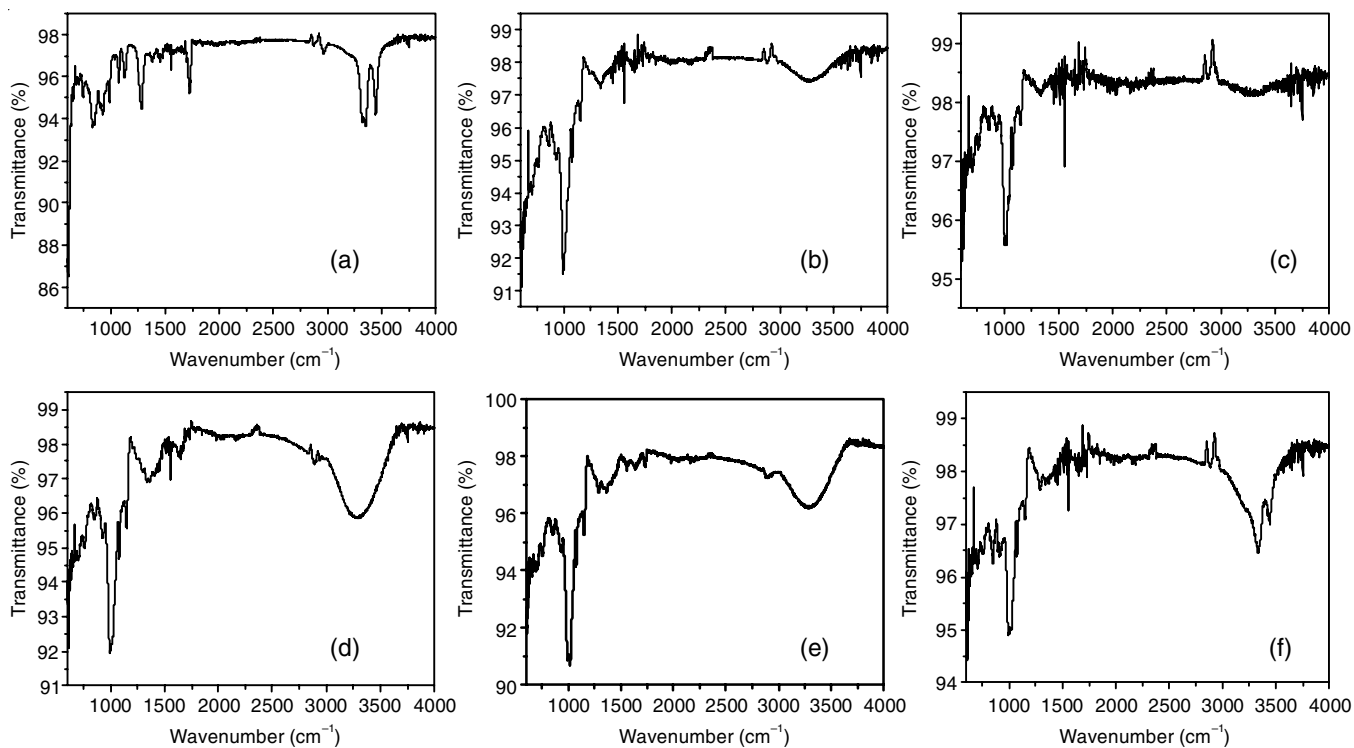


Fig. 2. FT-IR spectra of (a) CuO nanoparticles; (b) standard starch; (c) rice starch; (d) CuO-starch nanocomposites from copper acetate; (e) CuO-starch nanocomposites from copper chloride and (f) CuO-starch nanocomposites from equimolar mixture of copper acetate and copper chloride

TABLE-1
FT-IR REPRESENTING THE WAVENUMBERS AND CORRESPONDING CHEMICAL BONDS OF CuO-STARCH NANOCOMPOSITES

Wavenumber (cm ⁻¹)	Bonds	Compounds					
		A	B	C	D	E	F
3200-3700 ^{bm}	O-H stretching of glucopyranose ring in starch	–	3274	3299	3287	3287	3219
3000-2840 ^w	Assymmetric stretching of C-CH ₂ -C present in glucose	–	2885	2887	2889	2901	2988
1650-1580 ^w	O-H deformation of an inbonded water molecule in starch	–	1646	1646	1647	1642	1646
1600-1200 ^w	C-H and O-H bending of -CH ₂ and -OH Group	–	1339	1340	1340	1366	1293
1158 ^w	C-O stretching of C-OH bond of starch	–	1148	1152	1149	1149	1149
1080 ^w	Stretching vibration of C-O-C	–	1076	1079	1076	1079	1077
1000 ^s	Attributed to amylose and amylopectin of starch	–	995	1018	995	1018	995
926 ^w	Intramolecular bonding of the -OH group located in the C-6 position	–	915	925	924	923	916
1000-700 ^w	Stretching of Cu-O	837	–	–	843	845	847

A: CuO nanoparticles; B: Standard starch; C: Rice starch; D: CuO-starch nanocomposites from copper acetate; E: CuO-starch nanocomposites from copper chloride and F: CuO-starch nanocomposites from equimolar mixture of copper acetate and copper chloride

also appeared at 1366-1293 cm⁻¹ (Fig. 2a-f). According to a recent study, the bands at 1600-1200 cm⁻¹ can be attributed to both the C-H bending of -CH₂ and the bending of -OH groups connected to the alcohol functional groups [20].

The major adsorption band arising from starch can be observed at 1200-1000 cm⁻¹. In the synthesized compounds, the peak at 1152-1148 cm⁻¹ due to the C-O stretching of C-OH bond and 1077-1076 cm⁻¹ stretching vibration of the C-O-C of starch. Present study data was confirmed with the previously published data. Previous data suggested that the absorption bands at 1300-1000 cm⁻¹ in starch, resulting from the stretching and bending vibrations of C-OH, skeletal vibrations of C-O-C bonds contributed by glycosidic linkages and stretching of the C-O and C-C [21]. Four characteristic absorption peaks appearing in the fingerprint region (*i.e.* between 1120 and 920 cm⁻¹) are due to skeletal vibrations of pyranose rings. The peaks at 1081 cm⁻¹ and 1158 cm⁻¹ are respectively attributed to the C-O-C and C-C stretching vibrations of anhydroglucose rings and particularly from the C-OH groups of starch [22,23]. The intense band observed at 1018-995 cm⁻¹ can be attributed to the presence of amylose and amylopectin in starch of the synthesized CuO-starch nanocomposites and the literature data also suggested that the IR band between 1050-950 cm⁻¹ indicating the amorphous character and crystalline order of starch [15,24, 25].

A band at 926-915 cm⁻¹ can be attributed to the intramolecular bonding of the -OH group located in the C-6 position. This was only observed in native starches due to its hydrophilicity and the presence of another band at the region 847-837 cm⁻¹ suggested the stretching of Cu-O. Thus on the basis of FT-IR data and comparison with the previous published data, the results showed that the isolated rice starch was pure and

existence of Cu-O bond in the composites showed that the CuO-starch nanocomposites were formed.

XRD studies: The characteristic diffraction peaks at 17.09°, 23.50° and 17.34°, 23.76° were observed in the XRD for the standard starch and isolated rice starch, respectively. The XRD diffraction peak of synthesized CuO-starch nanocomposites using 0.2 M Cu(CH₃COO)₂·2H₂O and 8 M NaOH as precursors occurs at 20.40°, 35.53°, 38.90° and 66.05°, while the CuO-starch nanocomposites using 0.2 M CuCl₂·2H₂O and 8 M NaOH as precursors showed the diffraction peaks at 19.80°, 35.56°, 38.60° and 66.12°. On the other hand, the CuO-starch nanocomposites synthesized using equimolar mixture of 0.2 M Cu(CH₃COO)₂·2H₂O and 0.2 M CuCl₂·2H₂O, 8 M NaOH as precursors showed the diffraction peaks at 16.38°, 17.76°, 31.71°, 32.36°, 39.76° and 50.17°. According to published data [15,17, 26], starch molecules are classified into A, B and C types based on crystallinity. XRD technique helps identify starch samples from their XRD peak patterns. Rice starch has a characteristic typical A-type polymorph (crystallite pattern) with single diffraction peak at 15-16°, doublet at 18-20° and a less intense peak 22-23°. Compared with the previous data, present result showed slight differences in the XRD patterns of rice starch, with all of the CuO-starch nanocomposites exhibiting a similar set of XRD peaks (Table-2). The reported X-ray diffraction patterns of the CuO nanoparticles at 35.58° and 38.78° was attributed to the formation of CuO monoclinic phase [27,28]. These results confirmed that the CuO nanoparticles were present in the CuO-starch nanocomposite synthesized by present approach and did not exhibit the low crystallinity diffraction peaks of starch as shown in Fig. 3a-f. However, the average crystallite sizes of rice starch and CuO-starch nanocomposites were calculated by using Debye-Scherrer's equation. Therefore,

TABLE-2
CRYSTALLITE SIZE, Z-AVERAGE SIZE AND ZETA POTENTIAL OF CUO-STARCH NANOCOMPOSITES

Nanocomposites	XRD crystallite size (nm)	Zeta sizer		
		Z-average size (nm)	PDI	Zeta potential (mV)
Standard starch	3.01	1260	0.93	-0.15
Rice starch	2.42	8770	0.90	1.35
CuO-starch NCs from copper acetate	3.13	1421	0.33	-2.07
CuO-starch NCs from copper chloride	6.46	1504	0.32	1.65
CuO-starch NCs from equimolar mixture of copper acetate and copper chloride	17.42	1796	0.36	-0.17

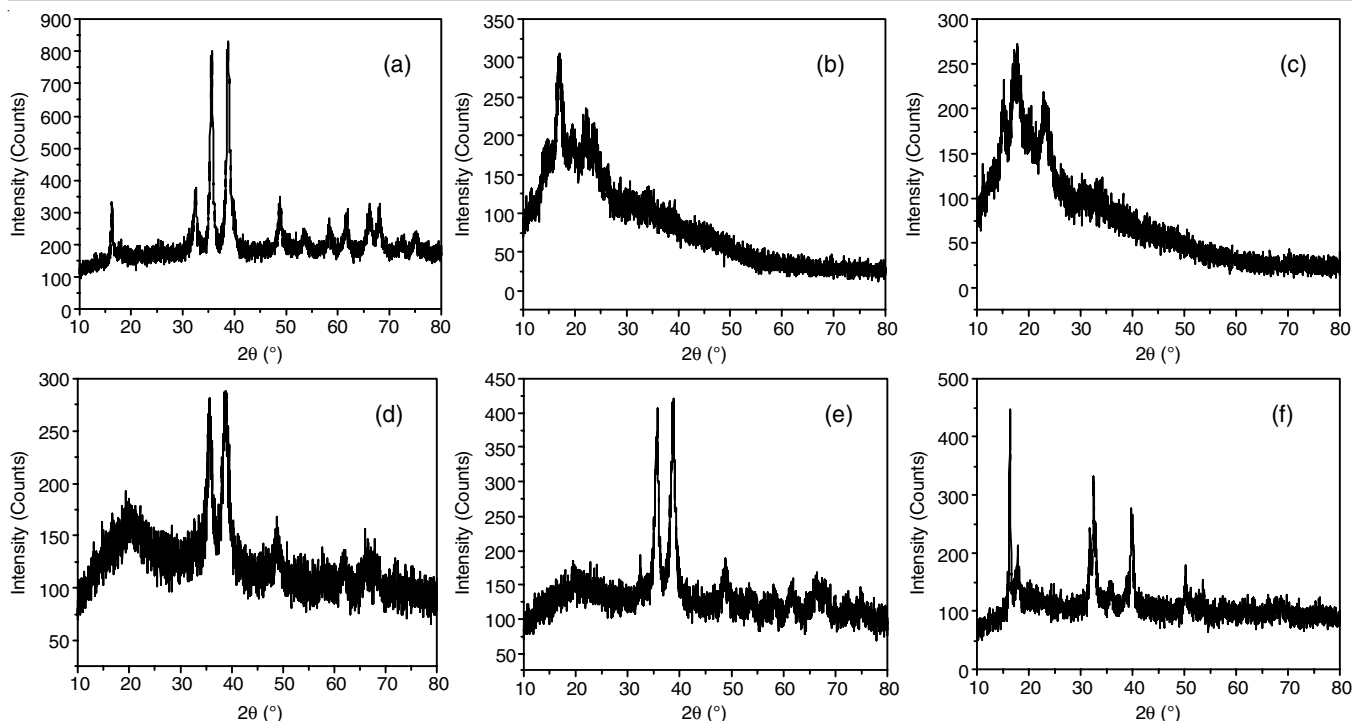


Fig. 3. XRD spectra of (a) CuO nanoparticles; (b) standard starch; (c) rice starch; (d) CuO-starch nanocomposites from copper acetate; (e) CuO-starch nanocomposites from copper chloride and (f) CuO-starch nanocomposites from equimolar mixture of copper acetate and copper chloride

the average crystallite size of standard starch and rice starch were calculated to be 3.01 nm and 2.42 nm, respectively. While the crystallite size of CuO-starch nanocomposites from different precursors *viz.* 0.2 M $\text{Cu}(\text{CH}_3\text{COO})_2 \cdot 2\text{H}_2\text{O}$, 0.2 M $\text{CuCl}_2 \cdot 2\text{H}_2\text{O}$ and equimolar mixture of 0.2 M $\text{Cu}(\text{CH}_3\text{COO})_2 \cdot 2\text{H}_2\text{O}$, 0.2 M $\text{CuCl}_2 \cdot 2\text{H}_2\text{O}$ were calculated as 3.13 nm, 6.46 nm and 17.42 nm, respectively (Table-2).

Zeta potential: The average particle size, zeta potential and particle size distribution of starch and CuO-starch nanocomposites are shown in Table-2. The average particle size

diameter of standard starch, rice starch, CuO-starch nanocomposite from copper acetate, CuO-starch nanocomposite from copper chloride and CuO-starch nanocomposite from equimolar mixture of copper acetate and copper chloride was found to be 1260, 8770, 1421, 1504 and 1796 nm, having poly dispersity index of 0.93, 0.90, 0.33, 0.32 and 0.36 with zeta potential value of -0.15, 1.35, -2.07, 1.65 and -0.17 mV, respectively. Moreover, the zeta potential of all starches and nanocomposites were found to be positive and negative (Figs. 4 and 5). Zeta potential predicts the long-term stability of the nanocomposites.

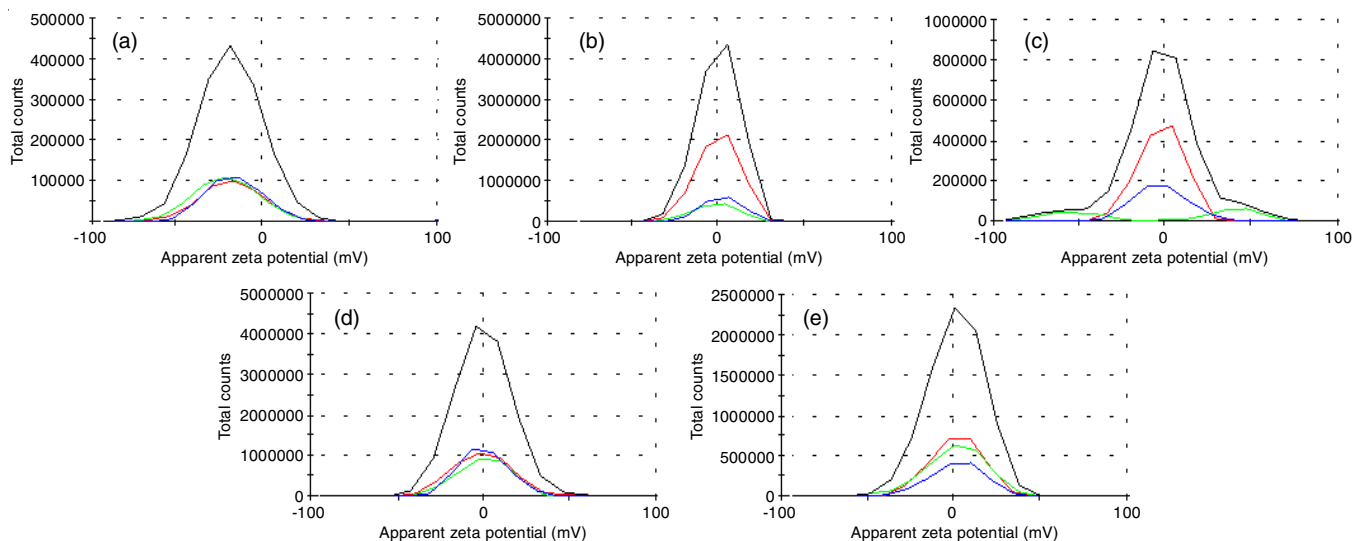


Fig. 4. Zeta potential distribution of starch and CuO-Starch nanocomposites [(a) standard starch; (b) rice starch; (c) CuO-starch nanocomposites from copper acetate; (d) CuO-starch nanocomposites from copper chloride and (e) CuO-starch nanocomposites from equimolar mixture of copper acetate and copper chloride]

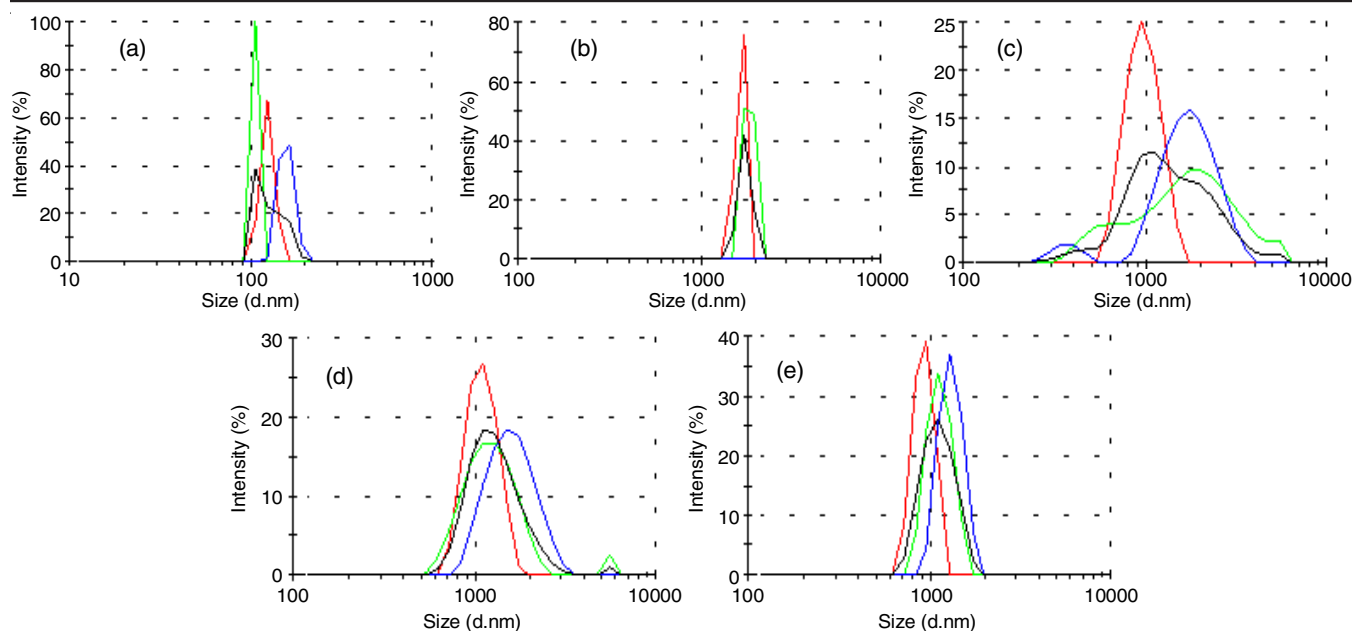


Fig. 5. Zeta size distribution of starch and CuO-starch nanocomposites [(a) standard starch; (b) rice starch; (c) CuO-starch nanocomposites from copper acetate; (d) CuO-starch nanocomposites from copper chloride and (e) CuO-starch nanocomposites from equimolar mixture of copper acetate and copper chloride]

The CuO-starch nanocomposite from copper acetate displayed significantly higher negative zeta potential (-2.07 mV) making them more stable than other CuO-starch nanocomposites synthesized by different precursor [24,29]. However, slight aggregation of the nanocomposite particles was observed in the synthesized nanocomposites.

Thermal analysis of CuO-starch nanocomposites

TGA analysis: Thermal decomposition of nonocomposite was analyzed by TGA and the thermograms of starch, CuO-starch nanocomposites (temperature range 32 to 700 °C) are shown Fig. 6. The first decomposition curve of all the three nanocomposites attributed due to the evaporation/dehydration

of absorbed and abounded water and the volatile compounds that starts immediately when the temperature rises and finishes below 100 °C, followed by the stability of anhydrous compounds. The second weight loss step (200-350 °C) corresponds to thermal decomposition in the TGA due to the degradation of amylose, amylopectin chain degradation and pyrolysis of the organic matter. The TGA curves show that all CuO-starch nanocomposites are stable up to (200-250 °C) with the maximum degradation rate at 300 °C.

After the final stage of decomposition, the result showed that 61.93 and 49.34% weight loss was observed for the CuO-starch nanocomposites synthesized from the precursor copper acetate and copper chloride, respectively (Table-3), while the

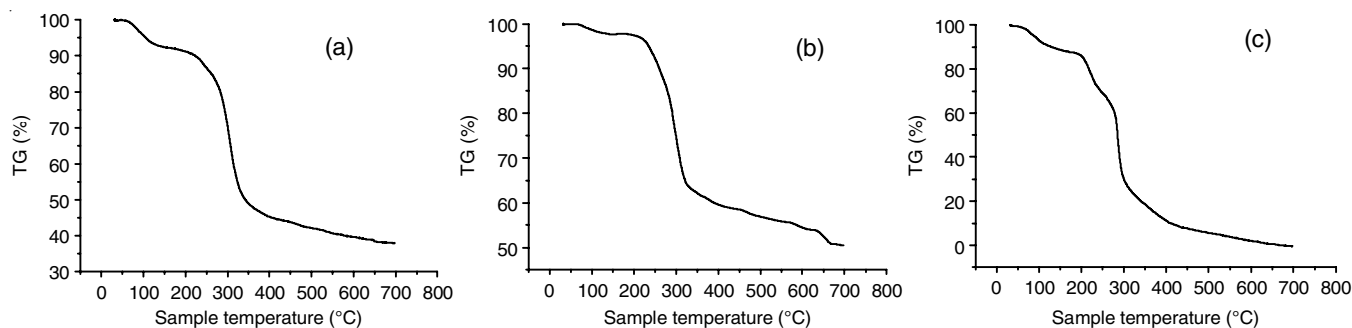


Fig. 6. TGA of starch and CuO-starch nanocomposites: (a) CuO-starch nanocomposites from copper acetate; (b) CuO-starch nanocomposites from copper chloride and (c) CuO-starch nanocomposites from equimolar mixture of copper acetate and copper chloride

TABLE-3
TGA OF CuO-STARCH NANOCOMPOSITES

Sample	ΔT (°C)	Decomposed mass ($\Delta m, \%$)	Remaining mass (%)
CuO-starch NCs from copper acetate	32.27-695.71	61.93	37.92
CuO-starch NCs from copper chloride	32.84-698.11	49.34	50.50
CuO-starch NCs from equimolar mixture of copper acetate and copper chloride	32.27-698.25	100.00	0.00

100% decomposition was observed in the nanocomposites synthesized from the equimolar mixture of copper acetate and copper chloride. The results indicate that CuO-starch nanocomposites were thermally stable and nanocomposite synthesized from copper chloride precursor was more stable with the higher residual content (50.5%) than the other nanocomposites synthesized from different precursor. Higher thermal stability can be attributed to the interactions with the nanocomposite surface and polymer matrix, consistent with the crystallinity of XRD results and other studies [30,31].

DSC analysis: Differential scanning calorimeter (DSC) was used to study the thermal stability and degradation of CuO-starch nanocomposites. The transition temperatures of the nanocomposites were recorded in order to obtain onset (T_o), offset (T_c) and peak (T_p) values. The onset (T_o), offset (T_c), peak (T_p) and enthalpy values for the CuO-starch nanocomposites obtained from different precursor are shown in Table-4. DSC thermogram of CuO-starch nanocomposites shows the two to three steps degradation (Fig. 7). DSC analysis showed endothermic peak between 50-100 °C for nanocomposites due to the dehydration. Endothermic peak could be attributed to the evaporation of surface water. In first step decomposition of all the nanocomposites, the transition temperatures ranged from 47.39-166.43 °C (T_o) and 109.71-232.34 °C (T_c), whereas the endothermic peak (T_p) ranged from 74.72-201.17 °C. The highest T_p was for the CuO-starch nanocomposite obtained from the copper chloride precursor and the lowest T_p was for the CuO-starch nanocomposites obtained from equimolar mixture of copper acetate and copper chloride with the endothermic enthalpy (ΔH) values were 75.81 J/g and 178.27 J/g, respectively. In

second step, decomposition the highest endothermic peak (T_p) at 266.27 °C was found for the CuO-starch nanocomposite obtained from copper chloride precursor with the endothermic enthalpy (ΔH) values were 48.80 J/g. Heat curves of DSC showed that third step decomposition only in the CuO-starch nanocomposite obtained from equimolar mixture of copper acetate and copper chloride precursor with the endothermic peak (T_p) at 282.48 °C and endothermic enthalpy (ΔH) value was 89.30 J/g.

The DSC plots provide complete information about the transition temperature changes of nanocomposites. The phase transition behaviour depends on the type of precursors used to obtain the CuO-starch nanocomposites. Successive structural changes resulted in gradual differences in endothermic patterns from low to high temperatures. The thermal properties studied using the DSC suggested that nanocomposites were semi-crystal structure. The peaks present between 200-300 °C due to the melting of crystallized amylopectin and co-crystallized amylose present in starch. The CuO nanoparticles may be form chemical bonds on hydroxyl group sites of the starch chains and the degradation of nanocomposites was affected by the CuO reinforced in the starch. The crystallinity of the nanocomposites depended on the interfacial interactions between the CuO nanoparticles and the amorphous part of the starch chains.

Antibacterial activity: The antibacterial activity data of synthesized CuO-starch nanocomposites against two bacteria are presented in Table-5. A solution of ampicillin having concentration 5 mg/mL was used as reference antibiotic. The CuO-starch nanocomposite showed significant antibacterial activity against two tested bacterial organisms. The higher inhibition

TABLE-4
DSC OF CuO-STARCH NANOCOMPOSITES

Sample	No. of step	Onset temp. T_o (°C)	Peak temp. T_p (°C)	Offset temp. T_c (°C)	$\Delta T = T_c - T_o$ (°C)	ΔH (J/g)
(a)	1	47.39	80.53 (Endo)	109.71	62.32	179.69
	2	250.25	266.27 (Endo)	285.28	35.03	48.80
(b)	1	166.43	201.17 (Endo)	232.34	65.91	75.81
	2	255.87	265.62 (Endo)	275.87	20.00	18.12
(c)	1	47.10	74.72 (Endo)	98.42	51.32	178.27
	2	187.30	212.23 (Endo)	235.44	48.14	135.80
	3	275.54	282.48 (Endo)	290.74	15.20	89.30

(a): CuO-starch nanocomposites from copper acetate; (b): CuO-starch nanocomposites from copper chloride and (c): CuO-starch nanocomposites from equimolar mixture of copper acetate and copper chloride

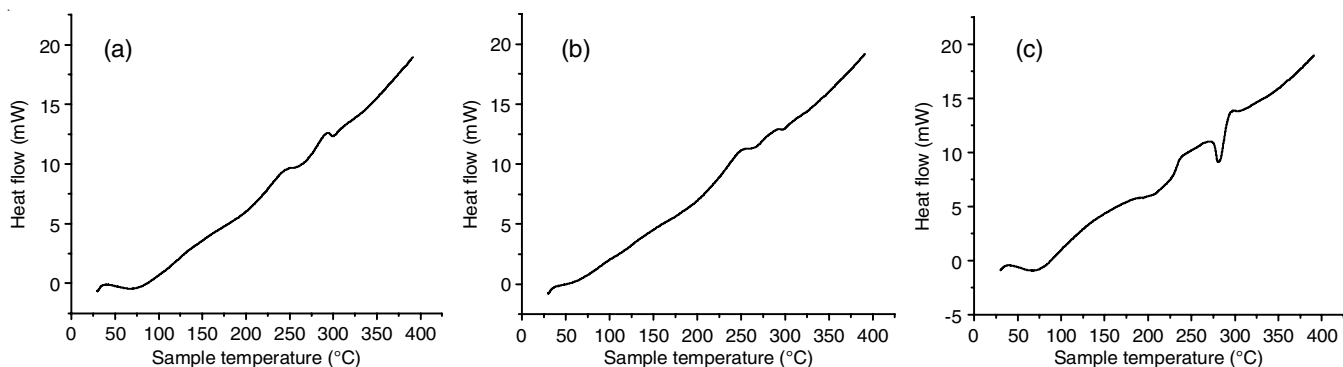


Fig. 7. DSC of starch and CuO-Starch nanocomposites: (a) CuO-starch nanocomposites from copper acetate; (b) CuO-starch nanocomposites from copper chloride and (c) CuO-starch nanocomposites from equimolar mixture of copper acetate and copper chloride

TABLE-5
ANTIBACTERIAL POTENTIAL OF CuO-STARCH NANOCOMPOSITES

Sample	Zone of inhibition (ZOI, mm)	
	<i>Escherichia coli</i>	<i>Serratia marcescens</i>
CuO-starch NCs from copper acetate	16.00 ± 0.58	17.00 ± 1.70
CuO-starch NCs from copper chloride	16.30 ± 0.30	15.67 ± 0.30
CuO-starch NCs from equimolar mixture of copper acetate and copper chloride	15.60 ± 0.30	17.67 ± 0.90
Ampicillin (Reference antibiotic)	9.00 ± 0.30	11.33 ± 0.30

*Values are mean (n = 3) ± standard error

zone was observed for the composite containing copper acetate precursor for the bacterial strains *S. marcescens* 17.67 ± 0.90 mm and for bacterial strain *E. coli* the higher zone of inhibition for the nanocomposite prepared by copper chloride 16.3 ± 0.30 mm. The antibacterial properties of CuO nanoparticles may be due to the interaction of the rice grain-like nanoparticles with the bacterial surface, which easily causes cell damage by disrupting the bacterial cell wall [32]. The antibacterial activity of metal nanoparticles depends on several factors, including ROS formation, cation release and cell wall damage. The efficiency of CuO nanoparticles depends on the concentration, stability and particle size. This facilitates the crossing of particles from bacteria cell membrane and subsequent destruction of key bacterial enzymes [33,34]. The observed good activity against bacteria may be due to the generation of ROS from the CuO-starch nanocomposites and cell damage of studies bacteria.

Conclusion

Copper oxide-starch nanocomposites were synthesized and characterized with the microscopic and spectroscopic techniques. The FT-IR data and SEM images confirmed the formation of CuO-starch bionanocomposites. The XRD analysis confirmed that CuO nanoparticles were present in the CuO-starch nanocomposite. Furthermore, the zeta potential and thermal analysis using TGA and DSC predicts the long-term stability of nanocomposites. Antibacterial assays indicated that the synthesized CuO-starch nanocomposites have significant antimicrobial activity against *S. marcescens* and *E. coli* and seem to be promising environment-friendly nanocomposites for antimicrobial applications in the different industries.

ACKNOWLEDGEMENTS

The authors thanks the Indian Institute of Technology, Delhi, Jamia Milia Islamia University, Delhi and the Indian Institute of Technology, Roorkee, India for providing the instrumental facilities. The authors are thankful to Prof. Raj N. Mehrotra, ex-Professor, Jodhpur University and Dr. Azad Jamia Milia Islamia University, Delhi and Dr. Ravindra Pandey, Assist. Prof., IIT Roorkee for useful and valuable suggestions. At last, the authors are also thankful to Dr. Mukesh Samant, Department of Zoology, S.S.J. University, Almora, India for the evaluating the antibacterial activity.

CONFLICT OF INTEREST

The authors declare that there is no conflict of interests regarding the publication of this article.

REFERENCES

1. A. Ujic, S. Krejčikova, M. Nevoralova, A. Zhigunov, J. Dybal, Z. Krulis, P. Fulín, O. Nyc and M. Slouf, *Front. Mater.*, **7**, 9 (2020); <https://doi.org/10.3389/fmats.2020.00009>
2. S. Liu, X. Li, L. Chen, L. Li, B. Li and J. Zhu, *Int. J. Biol. Macromol.*, **104**, 1330 (2017); <https://doi.org/10.1016/j.ijbiomac.2017.05.174>
3. T. Jiang, Q. Duan, J. Zhu, H. Liu and L. Yu, *Adv. Ind. Eng. Polym. Res.*, **3**, 8 (2020); <https://doi.org/10.1016/j.aiepr.2019.11.003>
4. C.I. Idumah and C.M. Obele, *Surfaces Interfaces*, **22**, 100879 (2021); <https://doi.org/10.1016/j.surfin.2020.100879>
5. A.M. Nafchi, A.K. Alias, S. Mahmud and M. Robal, *J. Food Eng.*, **113**, 511 (2012); <https://doi.org/10.1016/j.jfoodeng.2012.07.017>
6. M.B. Gawande, A. Goswami, F.X. Felpin, T. Asefa, X. Huang, R. Silva, X. Zou, R. Zboril and R.S. Varma, *Chem. Rev.*, **116**, 3722 (2016); <https://doi.org/10.1021/acs.chemrev.5b00482>
7. S. Saran, G. Sharma, M. Kumar and M.I. Ali, *Int. J. Pharm. Sci. Res.*, **8**, 3887 (2017); [https://doi.org/10.13040/IJPSR.0975-8232.8\(9\).3887-92](https://doi.org/10.13040/IJPSR.0975-8232.8(9).3887-92)
8. G. Sharma, N.D. Jasuja, M. Kumar and M.I. Ali, *J. Nanotechnol.*, **2015**, 132675 (2015); <https://doi.org/10.1155/2015/132675>
9. A.K. Chatterjee, R.K. Sarkar, A.P. Chattopadhyay, R. Chakraborty, P. Aich and T. Basu, *Nanotechnology*, **23**, 085103 (2012); <https://doi.org/10.1088/0957-4484/23/8/085103>
10. S.V.P. Ramaswamy, S. Narendhran and R. Sivaraj, *Bull. Mater. Sci.*, **39**, 361 (2016); <https://doi.org/10.1007/s12034-016-1173-3>
11. J. Chen, B. Karmakar, M.A. Salem, A.Y. Alzahrani, M.Z. Bani-Fwaz, M.M. Abdel-Daim and A.F. El-Kott, *Arab. J. Chem.*, **15**, 103681 (2022); <https://doi.org/10.1016/j.arabjc.2021.103681>
12. V.C. Verma, A. Kumar, M.G.H. Zaidi, A.K. Verma, J.P. Jaiswal, D.K. Singh, A. Singh and S. Agrawal, *Int. J. Curr. Microbiol. Appl. Sci.*, **7**, 211 (2018); <https://doi.org/10.20546/ijcmas.2018.710.022>
13. J. Ma, W. Zhu, Y. Tian and Z. Wang, *Nanoscale Res. Lett.*, **11**, 200 (2016); <https://doi.org/10.1186/s11671-016-1404-y>
14. K. Dasila and M. Singh, *S. Afr. J. Bot.*, **145**, 177 (2022); <https://doi.org/10.1016/j.sajb.2021.07.020>
15. I. Govindaraju, G.Y. Zhuo, I. Chakraborty, S.K. Melanthota, S.S. Mal, B. Sarmah, V.J. Baruah, K.K. Mahato and N. Mazumder, *Food Hydrocoll.*, **122**, 107093 (2022); <https://doi.org/10.1016/j.foodhyd.2021.107093>
16. A. Musa, K. Hakan, K. Suumlleyman and S.K. Derya, *Afr. J. Biotechnol.*, **10**, 2867 (2011); <https://doi.org/10.5897/AJB10.1567>
17. P.V. Kowsik and N. Mazumder, *Microsc. Res. Tech.*, **81**, 1533 (2018); <https://doi.org/10.1002/jemt.23160>
18. J.M. Fang, P.A. Fowler, J. Tomkinson and C.A.S. Hill, *Carbohydr. Polym.*, **47**, 245 (2002); [https://doi.org/10.1016/S0144-8617\(01\)00187-4](https://doi.org/10.1016/S0144-8617(01)00187-4)
19. R. Kizil, J. Irudayaraj and K. Seetharaman, *J. Agric. Food Chem.*, **50**, 3912 (2002); <https://doi.org/10.1021/jf011652p>
20. A. Lopez-Rubio, J.M. Clarke, Ben Scherer, D.L. Topping and E.P. Gilbert, *Food Hydrocoll.*, **23**, 1940 (2009); <https://doi.org/10.1016/j.foodhyd.2009.01.003>

21. D. Fan, W. Ma, L. Wang, J. Huang, J. Zhao, H. Zhang and W. Chen, *Stärke*, **64**, 598 (2012); <https://doi.org/10.1002/star.201100200>
22. A. Hebeish, M.H. El-Rafie, M.A. El-Sheikh and M.E. El-Naggar, *J. Inorg. Organomet. Polym. Mater.*, **24**, 515 (2014); <https://doi.org/10.1007/s10904-013-0004-x>
23. M. Kacurakova and M. Mathlouthi, *Carbohydr. Res.*, **284**, 145 (1996); [https://doi.org/10.1016/0008-6215\(95\)00412-2](https://doi.org/10.1016/0008-6215(95)00412-2)
24. M. Ahmad, A. Gani, I. Hassan, Q. Huang and H. Shabbir, *Sci. Rep.*, **10**, 3533 (2020); <https://doi.org/10.1038/s41598-020-60380-0>
25. T.Y. Liu, Y. Ma, S.F. Yu, J. Shi and S. Xue, *Innov. Food Sci. Emerg. Technol.*, **12**, 586 (2011); <https://doi.org/10.1016/j.ifset.2011.06.009>
26. K. Piyada, S. Waranyou and W. Thawien, *Int. Food Res. J.*, **20**, 439 (2013).
27. W.-T. Yao, S.-H. Yu, Y. Zhou, J. Jiang, Q.-S. Wu, L. Zhang and J. Jiang, *J. Phys. Chem. B*, **109**, 14011 (2005); <https://doi.org/10.1021/jp0517605>
28. J. Prasad, V. Kumar, B. Chandra and N.D. Kandpal, *Rasayan J. Chem.*, **15**, 72 (2022); <https://doi.org/10.31788/RJC.2022.1516579>
29. B. Schafer, M. Hecht, J. Harting and H. Nirschl, *J. Colloid Interface Sci.*, **349**, 186 (2010); <https://doi.org/10.1016/j.jcis.2010.05.025>
30. S. Estevez-Areco, L. Guz, R. Candal and S. Goyanes, *Food Hydrocoll.*, **108**, 106054 (2020); <https://doi.org/10.1016/j.foodhyd.2020.106054>
31. K. Charoensri, C. Rodwihok, D. Wongratanaphisan, J.A. Ko, J.S. Chung and H.J. Park, *Polymers*, **13**, 425 (2021); <https://doi.org/10.3390/polym13030425>
32. A. Ananth, S. Dharaneedharan, M.S. Heo and Y.S. Mok, *Chem. Eng. J.*, **262**, 179 (2015); <https://doi.org/10.1016/j.cej.2014.09.083>
33. O. Mahapatra, M. Bhagat, C. Gopalakrishnan and K.D. Arunachalam, *J. Exp. Nanosci.*, **3**, 185 (2008); <https://doi.org/10.1080/17458080802395460>
34. A. Azam, A.S. Ahmed, M. Oves, M.S. Khan, S.S. Habib and A. Memic, *Int. J. Nanomedicine*, **7**, 6003 (2011); <https://doi.org/10.2147/IJN.S35347>